Supplementary material to:
Volcanic SO$_2$ and SiF$_4$ visualization and their ratio monitored using 2-D thermal emission spectroscopy

W. Stremme[1], A. Krueger[1,2], R. Harig[2], and M. Grutter[1]

[1]Centro de Ciencias de la Atmósfera, Universidad Nacional Autónoma de México, Mexico City
[2]Technische Universität Hamburg Harburg, Germany

Correspondence to: Michel Grutter (grutter@servidor.unam.mx)

1 Video animations of the SO$_2$ plume (in ppm·m)

The film *SO2_volcanic_plume.mpg* shows 3 sequences of the SO$_2$ plumes emitted to the atmosphere. All measurements are taken from Altzomoni at 4000 m a.s.l. and 12 km North of the Popocatepetl volcano (5465 m a.s.l.). The false-color images are calculated automatically with the GeDetekt software and in all cases the (plume-sky) retrieval method used the column in the left border as sky spectrum for the evaluation of the pixels in the corresponding row.

1.1 Part I (17 March 2006)

The first sequence of the video shows the volcano emitting SO$_2$ passively in rather windy conditions, when a wind speed of around 10 m/s at 500 hPa was recorded by a radiosonde launched at 12 LT (or 18 UT) from the airport 50 km NW of the volcano. It can be seen sometimes that the plume is separated downwind and that the wind direction depends on the altitude. Due to the rather fast propagation of the plume, the measured SO$_2$ columns remain moderate even though the volcano is quite active. The color-scale (black-blue-red-yellow-white) is not shown but covers the 0 to 1500 ppm m range (approx. 4E18 molec/cm^2). The relatively large wind speeds make the puffs leave the field of regard rather fast in this data set, making it difficult for automatically calculating the flux (see Section 3.3).

1

1.2 Part II (1-2 December 2007)

Night measurements of the volcanic SO_2 plume about half a day after a small eruption had taken place at 6:20 am LT (see Stremme et al. (2011)). This sequence shows more continuous and passive degassing conditions at moderate and rather constant wind speeds. Only small variations occur in these sequence but providing the necessary information for wind-field retrievals and flux calculations. Results in Figs 13. and 14 are calculated from two frames within this period.

1.3 Part III (16-17 November 2008)

The last sequence shows measurements also during the night but on 16-17 November 2008. There are frequent interruptions for radiometric calibrations and the validation described in Section S.4. As described in the text, a strong Vulcanian-type explosion occurred around 1:06 LT (7:06 UT), which happened during the shown sequence. The presence of ash, also shown as the white areas in Fig. 8, does not allow for the retrieval of the SO_2 columns and the plume is not seen in the animation because these pixels are colored in black by the software. At the edges of the measured window, however, large SO_2 column densities were evaluated. After the amount of ash had diminished (about 40 min. after the explosion), the strong light-colored SO_2 plume becomes evident. As the plume propagates towards the observation site, it presents a broad cone-like shape. The wind direction turned from SW at sun-set to the S two hours later or about midnight and again towards the SE at dawn, just before the animation stops. In this sequence , the color-scale covers the 0 to 2000 ppm m range (6E18 molec/cm^2). A quantification from this sequence may have larger uncertainties since it is not well known with what temperature the SO_2 is emitted during the explosion and how fast the emitted SO_2 gas adopts the environmental temperature with respect to the passively emitted SO_2 in most of the other cases.

2 Video animation of simultaneous SO_2 and SiF_4 in (ppm·m)

The simultaneous slant column distribution of the volcanic SO_2 and SiF4 gases emitted by Popocatépetl is presented in the file *SO2_SiF4.mpg*. This animation is intended to demonstrate small differences in the temporal and spatial evolution of both volcanic gases, which as has been shown in the article, are emitted in different proportions depending on the activity of the volcano.

An enhanced SiF_4 emission is assumed to be related with Vulcanian-type explosions (text of article, Francis et al. (1996), Love et al. (2000) and Stremme et al. (2011)). The animation shows the false-color images of SiF_4 and SO_2 of the night 16-17 November 2008, as well as the brightness temperature reflecting the spatially-resolved amount of IR radiation received by the instrument. The eruption at 7:06 UT is also shown in the article (Fig.9) and in the previous video (S.1). It is evident that both gases have a different relative evolution throughout this event as can be confirmed by the temporal SiF_4/SO_2 plot in Fig.9. The eruption itself lasted for about 40 minutes and it took some

2

more minutes until the ash separated from the gas plume. After the ash fell, the gas-plume appeared first at the top of the images. Later the SiF_4 plume slowly faded out while the SO_2 emission remained almost constant..

To suppress noise in the animation, the correlation coefficient between the SiF_4 reference spectrum to the measured spectra is used as threshold. All SiF_4 columns with values below 0.93 are set to 0. Since up to now no other eruptions have been recorded with an infrared gas imaging device, the experience in SiF_4-column measurements at 4 cm^{-1} is poor and a proper validation is missing. Therefore, the relatively change in the SiF_4 and not the absolute column values should be considered (see also text in the article).

60   3   Diagnostics of the wind-field retrieval

The data sets studied have measurement-specific variations in view of the image, time between the frames, step-size and radiometric calibration and are taken under different conditions in volcanic activity, wind-speed, wind shear etc. Therefore, the strength of the constraint has to be chosen for each data set individually with certain criteria. In this supplementary part we present the graphics

65   which are taken into account for evaluating the results as well as the graphics which visualize how the flux time.series are calculated.

The flux calculation is done in different steps and a set of automatically produced graphics allow for the visualization and quality control of the result. Figures S.1 and S.5 are more or less identical to Fig. 12 and 13 in the article. The quantity DOF (in the title of Figs. S.1 and S.2) is the trace of

70   a resolution matrix, which is calculated according to the averaging-kernel matrix well known from atmospheric profile retrievals (Rodgers,2000).

3.1   Solution of the inverse problem

Figures S.1 and S.2 describe the state of the atmosphere: wind-field, SO_2-column densities and SO_2 sources. How much information is used to describe the vector field has been chosen with the

75   constraint. Its number of elements describes the upper limit, the maximal independent pieces in this case would be 2142. In fact the degree of freedom of signal regarding the wind field has a much smaller value of DOFwind = 98.3 (equals to DOFall (421.91) - DOFSource (323.6)).
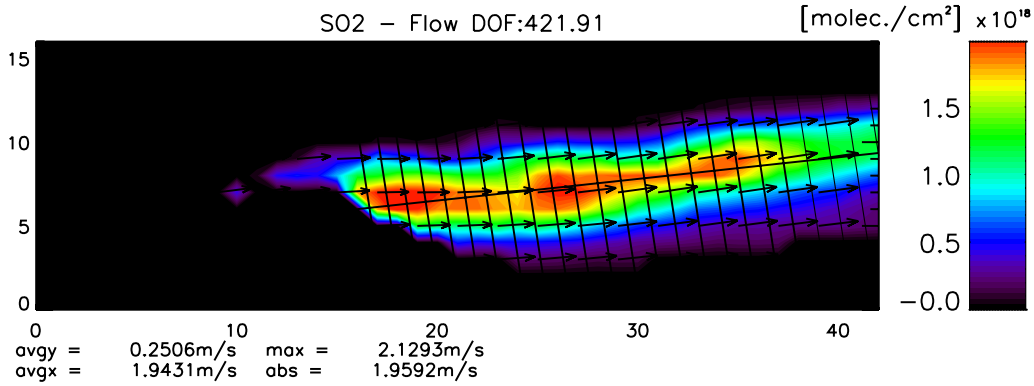

Fig. 1. Wind-field (arrows) obtained from the two sequential SO_2-frames using the column density (colored) information. The wind-field is the most important part of the solution vector in the ill-posed inverse problem.

3.2   Wind speed and flux rate

Figures S.3, S.4 and S.5 help to check and correct the averaged wind speed using cross-correlation.
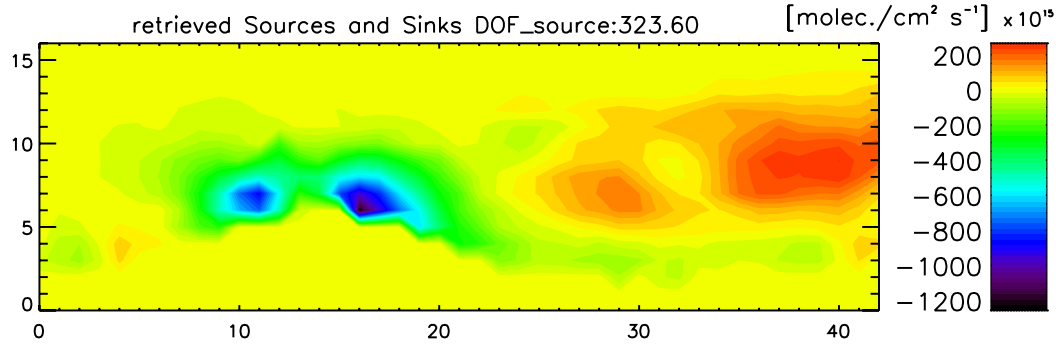
4

Fig. 2. Retrieved sources are also part of the solution vector. As the wind-field is rather strongly constrained, the additional fit-parameter improves the fit significantly. The free atmosphere is constrained with a smoothing constraint, while the pixels of the borders and the ground with the volcanic body are constrained with an optimal-estimation-like regularization (R-matrix is diagonal). In this example, 323.6 independent pieces of information are included in the vector which has 714 elements to describe the sources.
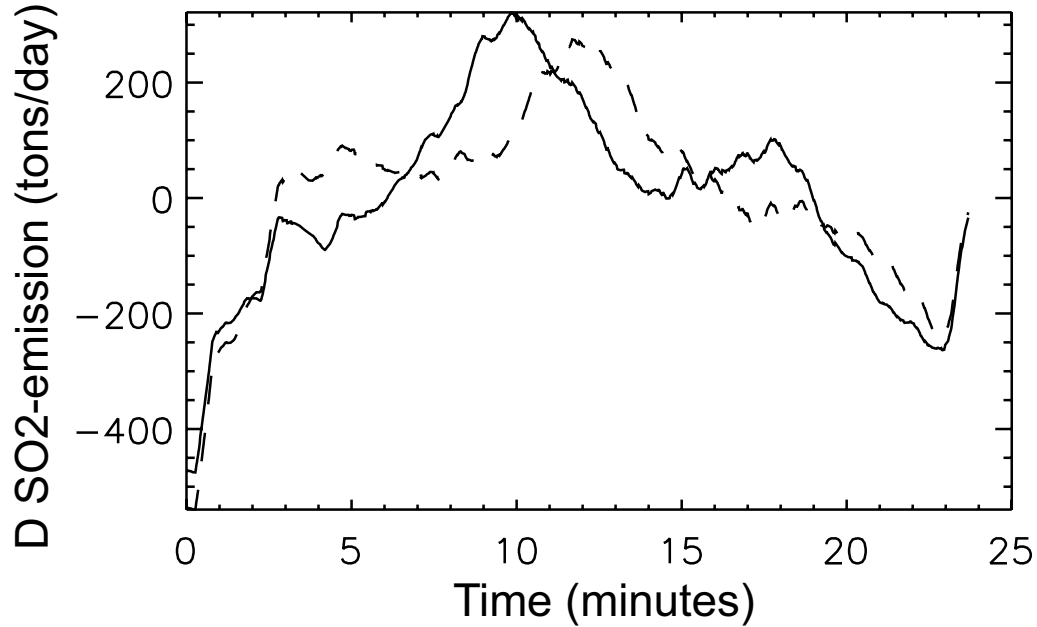

Fig. 3. Variation of the SO_2 flux as function of distance from the crater (here expressed as time). A fitted straight-line was subtracted from the obtained time-series in Fig. 13 in order to obtain this D-SO_2 plot. As mentioned, the SO_2 fluxes are calculated using the plume cross-sections showed as the black parallel lines perpendicular to the average direction of propagation in Fig S.1. The flux can be calculated using either the SO_2 column densities of the first (solid trace) or the second (dashed trace) frames. The time starts at the first cross-section in Fig. S.1 for both flux time series. Please note that the delay between the flux time-series of the first and second frames (calculated below) is corrected in Fig.13 of the article but not here.
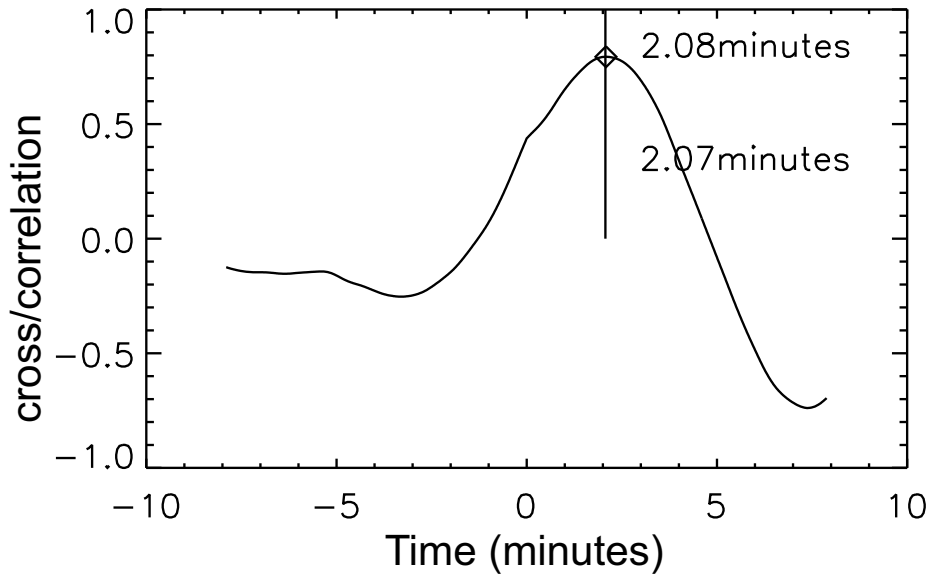
5

Fig. 4. The cross-correlation of the flux time-series in Fig. S.3 shows a maximum corresponding to the delay between both frames. If the wind field is well retrieved, the delay obtained from this cross-correlation (diamond at the maximum after 2.08 min) should coincide with the known time delay between both measured frames (vertical line at 2.07 min). Normally, a small difference could always be expected since the wind-field result is smoothed and it is assumed that the plume does not change its direction of propagation, but larger discrepancies in the delays would mean that the wind-fields have not properly been retrieved.
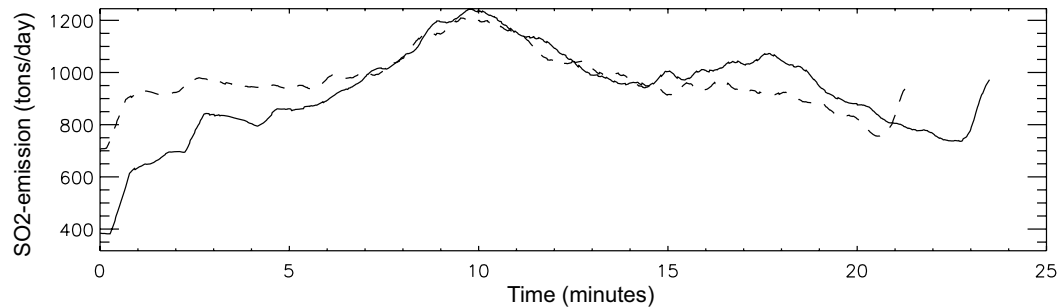

Fig. 5. Time-series of the fluxes after correcting the second frame by subtracting thes delay from Fig. S.4. This plot is equivalent to Fig. 13 and shows how both curves behave more similarly and the flux rate at the center of the plot seems to be reliable.

80 **3.3 Quality of the fit**

The goodness, describing how well the retrieved solution vector represents the recorded measurements, can be visualized by comparing Fig. S.6 with Fig. S.7 or looking directly at the difference of both shown in Fig. S.8. In analogy to spectroscopic retrievals, in this inverse problem reconstructing the wind-field in Figure S.1, Figs. S.6, S.7 and S.8 represent the observed, calculated and residual

6

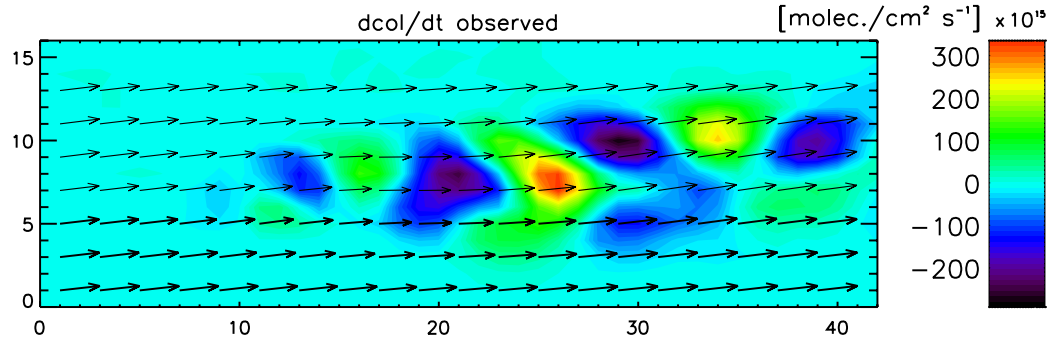85 vectors, respectively. The measurement (Fig. S.6) and the simulation (Fig. S.7) should be similar.

Fig. 6. False-color plot showing the rate how the observed columns change between the two consecutive frames (see Eq. 4 in the article) and represents the measured input vector for the reconstruction of the wind-field.
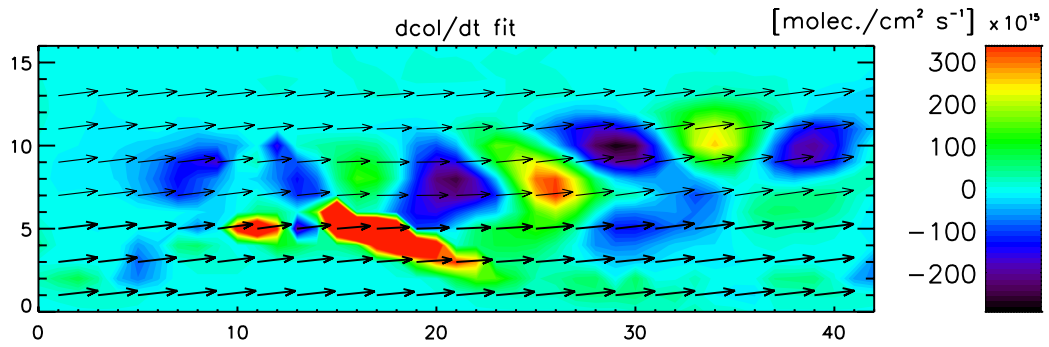

Fig. 7. False-color plot showing the rate how the simulated columns change between the two consecutive frames (same as Fig. S.6 but calculated using the solution vector, consisting of the retrieved vector field and the retrieved source filed).
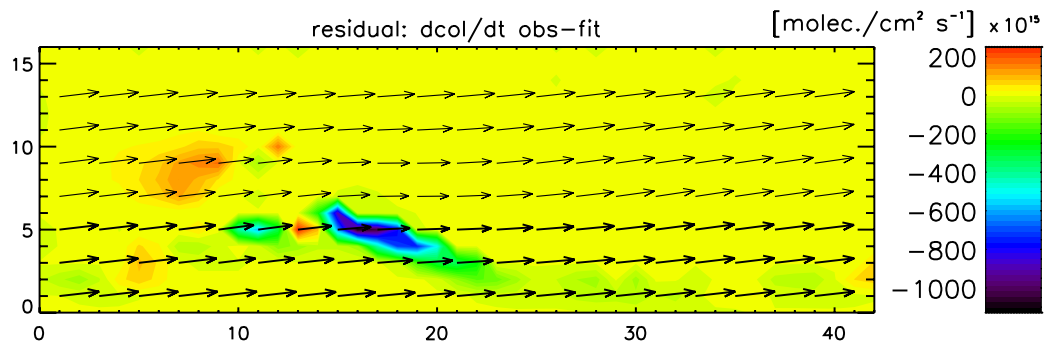

Fig. 8. False-color plot showing the difference between the measured (Fig. S.6) and simulated (Fig. S.7) column rates.

A good result (low residuals) is obtained throughout the observation window and particularly

7

where the plume is observed, but large residuals at the edge of the volcano occur systematically from different reasons: i) The wind-field is spatially smoothed with a constraint and cannot represent real propagation of the SO_2 plume near the body of the volcano very well. ii) The sources are constrained as well, but the constraint is different in the body of the volcano and the open atmosphere. iii) Those pixels where the SO_2 column retrieval presents a lower correlation than 0.93 are deweighted and therefore the pixels outside the plume have larger residuals.

4 Validation of SO$_2$ and SiF$_4$ 0.5 cm^{-1} retrievals from lunar absorption measurements

The results of SO$_2$ and SiF$_4$ slant columns retrieved form lunar absorption spectra (spot A in Fig. 1) are shown in Figure S.9. The analysis of the data was performed as from solar absorption spectra in Stremme et al. (2009). The measurements were taken on 17 November 2008 around 6:30 a.m. LST at when the moon had a zenith angle of 30 and an illumination fraction of 76%. The volcanic plume passed just above the observation site and it was possible to take absorption spectra for little less than an hour. As the thermal emission from the moon and that of the atmosphere including the volcanic plume have the same order of magnitude, background spectra just next to the moon were also recorded. These background spectra served rather to get slant columns in thermal emission mode since the plume was just above the measurement site. Figure S.10 shows that one of the lunar background measurements (a thermal emission spectrum) was recorded near the maximum of the slant columns retrieved from lunar absorption. Therefore, it is possible to subtract an individual background obtained by linear interpolation from the thermal emission spectra recorded before and afterwards.
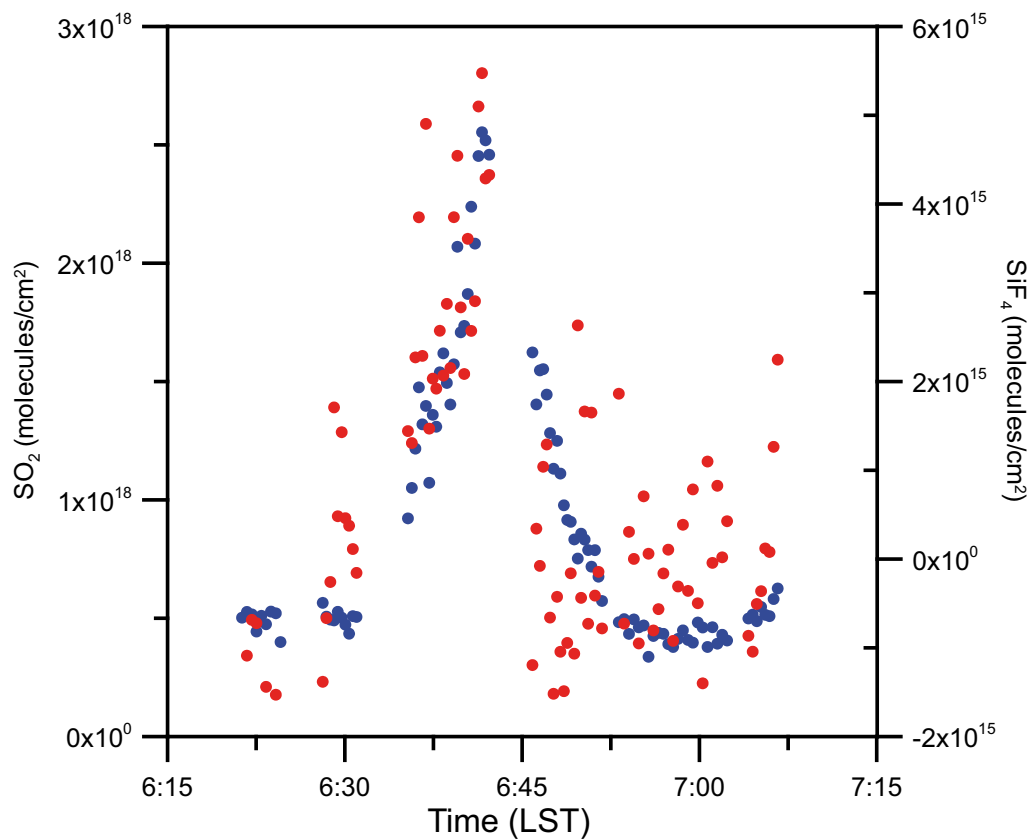

Fig. 9. Time-series of the SiF$_4$ (red) and SO$_2$ (blue) slant columns retrieved from lunar absorption spectra taken on 17 November 2008. Time is given in local time.

The first assumption of a volcanic plume temperature of 272 K lead to a systematic lower SO_2 column retrieved from thermal emission spectra than the temperature independent retrieval results from lunar absorption spectra (the blue triangle in Fig. S.10. is the lunar absorption value interpolated

110 to the time of the thermal emission measurement). The results of the sensitivity study in Section S.5 and Fig. S.11 shows a temperature of 266 K, for which both SO_2-slant columns are consistent. That is indicated by the green crosses (thermal emission) and blue triangle (interpolated lunar measurements) in Figure S.10. The plume temperature is a parameter which can be obtained from the comparison of both methods. The radiosonde at 17 November 2008, 6:00 am L.T. at Mexico City

115 registered a temperature of 265 K at 5000 m.a.s.l., which was the aprox. plume height. This result suggests that the volcanic plume seems to adapt rather fast to the temperature of the environment.
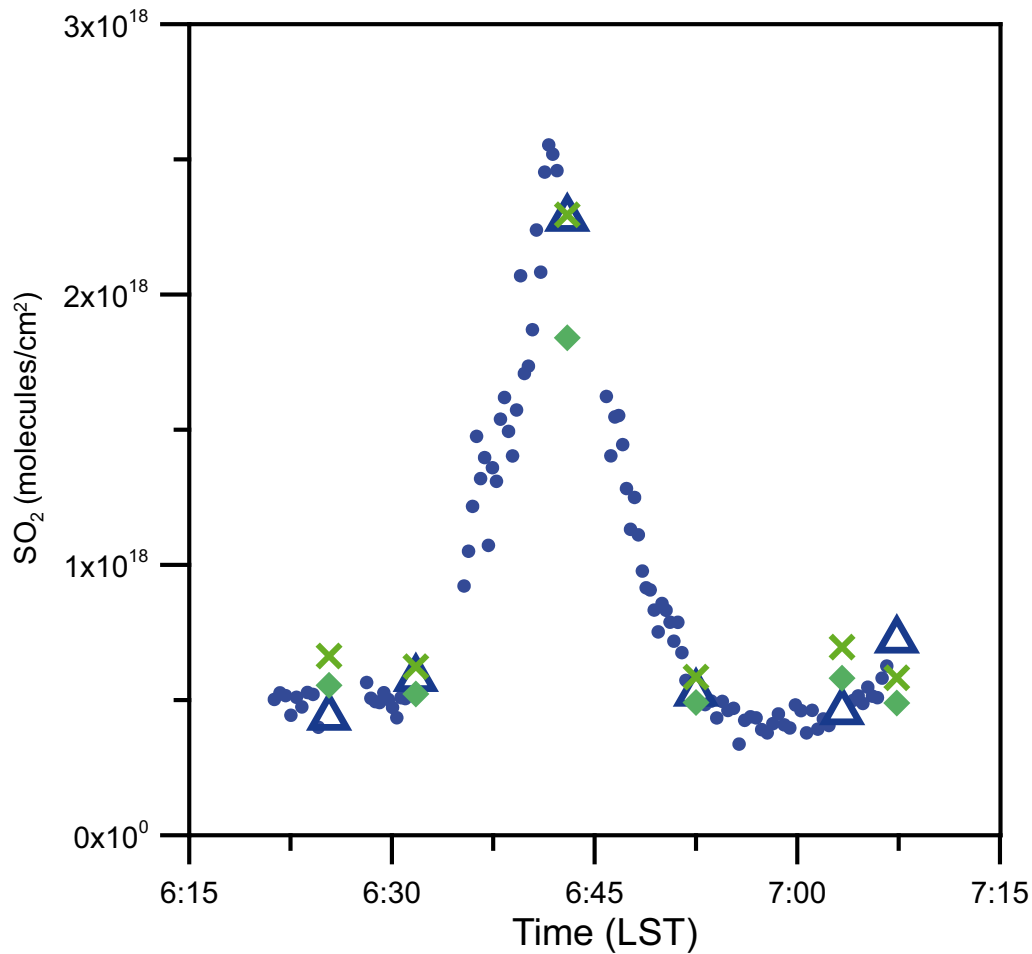

Fig. 10. SO_2 slant columns of SO_2 retrieved from lunar absorption spectra (blue) plotted together with SO_2 from thermal emission spectra at 0.5 cm^{-1} (green). The diamonds are results when a plume temperature is assumed to be 272 K and the crosses are after fitting the SO_2 columns to the lunar absorption value, giving a plume temperature of 266 K.

10

5   Diagnostic and estimation of systematic errors

Random errors of the retrieved columns can be estimated from the scattering of the results (Fig.9 of article) while in the calculation of ratios, the random error obtained from the 95% confidence intervals is small if enough spectra are recorded. However, various parameters in the forward model affect the results systematically and have to be discussed to evaluate the results and to improve future measurements.

5.1   Sensitivity to plume temperatures

The assumed plume temperature has a strong impact on the estimated slant columns, and is normally not measured directly. Love et al. (2000) limited their analysis by using molecular ratios of the volcanic gases and not the absolute slant column measurements, which would be needed for estimating the flux. They mentioned that from their analysis, the SiF_4/SO_2 ratio changes by less than 5% if a 20 K higher volcanic plume temperature is assumed. This is appreciated from a sensitivity study performed from our results in which although the changes in the retrieved slant columns can be rather large, the temperature dependence of the molecular ratio is much more unresponsive.

SO_2 and SiF_4 were analyzed for this evaluation assuming different plume temperatures from a set of six thermal emission spectra of the volcanic plume taken some distance down-wind from the crater, close to the position of the moon (position A in Fig. 1). As the moon-absorption measurements (see Section S.4) were performed at the same time and elevation angle, the volcanic-plume temperature could be estimated using the results from the sensitivity study and the moon-absorption quite accurately. This strategy is similar to using simultaneous COSPEC-measurements as described by Love et al. (2000), who used the SO_2 slant column from an independent technique for "calibrating" the thermal emission result. Other possibilities for estimating the temperature could be from strong saturated water lines or from the altitude of the volcanic-plume together with the assumption that it adopts the temperature of the environment at that altitude.

5.2   Estimation of errors

One of the most important error sources of the experimental set-up used in this work is the radiometric calibration of the spectrometer. The calibration changes according to the temperature of the instrument and detector during measurements and a calibration every hour would be desired. Thus, the calibration itself might introduce errors, as the condition in the field was not always optimal for this procedure. For example, the calibrations during the Nov/Dec 2007 campaign was not as frequent as in May 2009, although the available electrical power in the measurement site was not sufficient to raise the temperature of the black-body's resistance as high as in the previous study. The instrument was installed inside a building for the latter campaign looking for more steady conditions and thus the conditions were somewhat different.
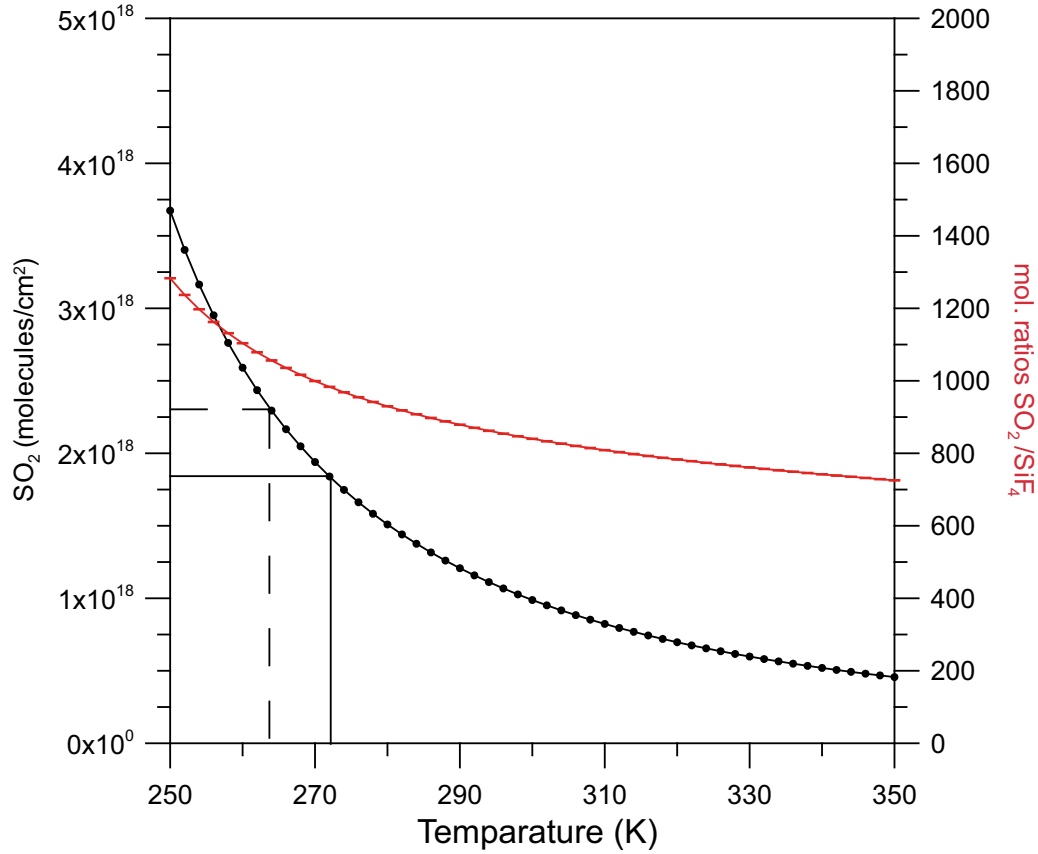
Fig. 11. Sensitivity of the retrieved SO_2 column to the estimated plume temperature (black points). The red line shows the resulting SiF_4/SO_2 molecular ratios as a function of chosen plume temperature. The ratios are obtained from the linear fit of the correlations of six spectra taken at 0.5 cm^{-1} resolution.

The error introduced by the calibration is evaluated assuming errors in both the upper and lower temperatures of the black-body measurements. Both temperature errors could have the same or opposite signs. If we assume an error of 1 K, the effect in the slant columns and ratios can be calculated. The radiometric calibration also affects the slant columns retrieved from a clear-sky spectrum. Table S.1 shows how the absolute slant-columns, the Δ slant-columns (plume-sky) and the calculated ratio between the ΔSiF_4 and SO_2 are affected. The error resulting from 1 K uncertainty in the temperatures of the black- bodies could lead to a 20% error in the SO_2/SiF_4 ratios.

The different errors shown in Table S.1 are important, if the method is applied to determine i) the absolute values of the slant column densities finally used for emission estimation or ii) the differences in the slant columns (sky-plume) are retrieved to calculate molecular ratios. As there are different fitting parameters (polynomials and interference gases) involved and the forward model is not linear, the error introduced through an error in the calibration does not behave equally for all target gases and do not compensate. The table shows that molecular ratios could be affected by as much of 22%,

12

Table 1. Sensitivity to calibration: Study with lunar-background measurements assuming a temperature of 273 K of the volcanic plume. The calibration temperatures were 284.45 and 292.55 K.

perturbation		1	2	3	4
δ Temp. cold		+1	0	+1	-1
δ Temp. hot		0	+1	+1	+1
δ SO2$_{max}$	molec./cm^2	-0.30E+18	0.02E+18	0.02E+18	0.67E+18
δ SO2$_{max}$	%	-17.2	1.2	1.2	38.7
δ SiF4$_{max}$	molec./cm^2	0.18E+15	-0.20E+15	-0.018E+15	-0.14E+15
δ SiF4$_{max}$	%	12.5	-14.2	-1.2	-9.7
$\delta(\Delta$ SO2)	molec./cm^2	-0.180E+18	0.018E+18	0.018E+18	0.422E+18
$\delta(\Delta$ SO2)	%	-14.8	1.5	1.5	34.7
$\delta(\Delta$ SiF4)	molec./cm^2	-0.21E+15	0.34E+15	0.023E+15	0.66E+15
$\delta(\Delta$ SiF4)	%	-18.9	30.7	2.1	59.6
$\delta(\Delta$ SO2/Δ SiF4)	molec./molec.	55.56	-244.50	-6.70	-170.07
$\delta(\Delta$ SO2/Δ SiF4)	%	5.09	-22.38	-0.61	-15.57

while a wrong calibration (1 K) might affect the column density by up to 60% for SiF$_4$ and up to 35% for SO$_2$.

The a priori slant partial columns and a priori values used for the interference parameters are empirically adjusted. Error through interference gases or fitted parameters are therefore one of the largest error sources in the retrievals. The error analysis in optimal estimation is described by Rodgers (1990), Bowman et al. (2006) and Sussmann and Borsdorff (2007). An important tool in the error analysis is the Averaging-Kernel matrix which describes how a change in one parameter x^j_{true} affects the result related to another parameter x^i_{ret}. For the parameters which are retrieved with a noticeable constraint, we define their average impact AI^{xxx}_j on the target gas, for example for the slant column of SO$_2$, as:

$$AI^{SO2}_j = A^{SO2}_j \cdot AVERAGE(x^j_{ret} - apriori) \tag{1}$$

represented by red bars in Fig. S.12. The variance in the impact SI^{xxx}_j is shown in blue and is given by:

$$SI^{SO2}_j = A^{SO2}_J \cdot STDEV(x^j_{ret}) \tag{2}$$

The plot in Fig. S.12. can be used to calibrate efficiently the retrieval by adjusting the interference parameters, a priori and constraint, so that the average of the volcanic gases in the clear-sky spectra (spot C in Fig.1 of the article) is effectively zero, while the target gases are almost freely adapted in the volcanic layer. The variance of the partly constraint interference parameter characterizes the retrieval as well.
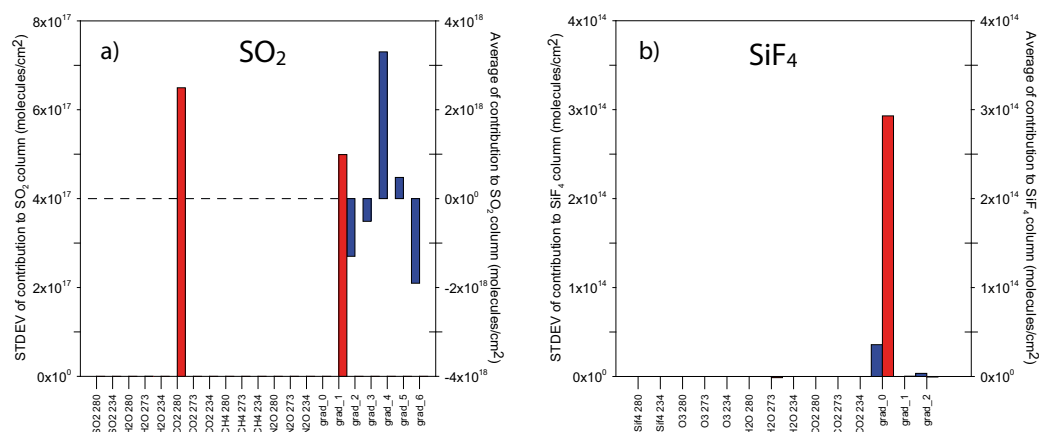
13

Fig. 12. Systematic errors introduced by the interference parameters in the case of (a) SO2 and (b) SiF$_4$ shown as responses in the retrieved slant columns (molec/cm^2). The average impact (blue) and the variance in the impact (red) are plotted as bars.

The optimization aimed to obtain zero values for the target gas in the clear-sky spectra, an overall well-fitted spectrum without a systematic residual within the plume, realistic average and STDEV
185 values of the interference parameters and an almost unconstrained fit of the target in the volcanic layer. An empirical adjustment of the parameter does not go in favor of the optimal estimation theory, but it is often not possible to obtain sufficient information about all possible interference-parameters for the slant columns.

References

190 Bowman, K. W., Rodgers, C. D., Kulawik, S. S., Worden, J., Sarkissian, E., Osterman, G., Steck, T., Lou, M., Eldering, A., Shephard, M., Worden, H., Lampel, M., Clough, S., Brown, P., Rinsland, C., Gunson, M., and Beer, R.: Tropospheric Emission Spectrometer: Retrieval Method and Error Analysis, IEEE Transactions on Geoscience and Remote Sensing, 44, 1297–1307, doi:10.1109/TGRS.2006.871234, 2006.

Francis, P., Chaffin, C., Maciejewski, A., and Oppenheimer, C.: Remote determination of SiF_4 in volcanic
195 plumes: A new tool for volcano monitoring, Geophys. Res. Lett., 23, 249–252, doi:10.1029/96GL00022, 1996.

Love, S. P., Goff, F., Schmidt, S. C., Counce, D., Pettit, D., Christensen, B., and Siebe, C.: Passive infrared spectroscopic remote sensing of volcanic gases: ground-based studies at White Island and Ruapehu, New Zealand, and Popocatépetl, Mexico, vol. 116 of *Geophys. Monogr.*, pp. 117–138, Am. Geophys. Union,
200 2000.

Rodgers, C. D.: Characterization and error analysis of profiles retrieved from remote sounding measurements, J. Geophys. Res., 95, 5587–5595, 1990.

Stremme, W., Ortega, I., and Grutter, M.: Using ground-based solar and lunar infrared spectroscopy to study the diurnal trend of carbon monoxide in the Mexico City boundary layer, Atmospheric Chemistry & Physics,
205 9, 8061–8078, 2009.

Stremme, W., Ortega, I., Siebe, C., and Grutter, M.: Gas composition of Popocatépetl Volcano between 2007 and 2008: FTIR spectroscopic measurements of an explosive event and during quiescent degassing, Earth and Planetary Science Letters, 301, 502–510, doi:10.1016/j.epsl.2010.11.032, 2011.

Sussmann, R. and Borsdorff, T.: Technical Note: Interference errors in infrared remote sounding of the atmo-
210 sphere, Atmospheric Chemistry and Physics, 7, 3537–3557, doi:10.5194/acp-7-3537-2007, 2007.

15